THE ASTROPHYSICAL JOURNAL, 493:955–969, 1998 February 1

TURBULENT COMPRESSIBLE CONVECTION WITH ROTATION. II. MEAN FLOWS AND DIFFERENTIAL ROTATION

NICHOLAS H. BRUMMELL
JILA and Department of Astrophysical and Planetary Sciences, University of Colorado, Boulder, CO 80309-0440
NEAL E. HURLBURT
Lockheed Martin Solar and Astrophysics Laboratory, Org 91-30, Building 252, 3251 Hanover Street, Palo Alto, CA 94304
AND
JURI TOOMRE
JILA and Department of Astrophysical and Planetary Sciences, University of Colorado, Boulder, CO 80309-0440
Received 1997 February 20; accepted 1997 September 11

ABSTRACT

The effects of rotation on turbulent, compressible convection within stellar envelopes are studied through three-dimensional numerical simulations conducted within a local *f*-plane model. This work seeks to understand the types of differential rotation that can be established in convective envelopes of stars like the Sun, for which recent helioseismic observations suggest an angular velocity profile with depth and latitude at variance with many theoretical predictions. This paper analyzes the mechanisms that are responsible for the mean (horizontally averaged) zonal and meridional flows that are produced by convection influenced by Coriolis forces. The compressible convection is considered for a range of Rayleigh, Taylor, and Prandtl (and thus Rossby) numbers encompassing both laminar and turbulent flow conditions under weak and strong rotational constraints.

When the nonlinearities are moderate, the effects of rotation on the resulting laminar cellular convection leads to distinctive tilts of the cell boundaries away from the vertical. These yield correlations between vertical and horizontal motions that generate Reynolds stresses that can drive mean flows, interpretable as differential rotation and meridional circulations. Under more vigorous forcing, the resulting turbulent convection involves complicated and contorted fluid particle trajectories, with few clear correlations between vertical and horizontal motions, punctuated by an evolving and intricate downflow network that can extend over much of the depth of the layer. Within such networks are some coherent structures of vortical downflow that tend to align with the rotation axis. These yield a novel turbulent alignment mechanism, distinct from the laminar tilting of cellular boundaries, that can provide the principal correlated motions and thus Reynolds stresses and subsequently mean flows. The emergence of such coherent structures that can persist amidst more random motions is a characteristic of turbulence with symmetries broken by rotation and stratification. Such structure is here found to play a crucial role in defining the mean zonal and meridional flows that coexist with the convection. Though they are subject to strong inertial oscillations, the strength and type of the mean flows are determined by a combination of the laminar tilting and the turbulent alignment mechanisms. Varying the parameters produces a wide range of mean motions. Among these, some turbulent solutions exhibit a mean zonal velocity profile that is nearly constant with depth, much as deduced by helioseismology at midlatitudes within the Sun. The solutions exhibit a definite handedness, with the direction of the persistent mean flows often prescribing a spiral with depth near the boundaries, also in accord with helioseismic deductions. The mean helicity has a profile that is positive in the upper portion of the domain and negative in the lower portion, a property bearing on magnetic dynamo processes that may be realized within such rotating layers of turbulent convection.

Subject headings: convection — stars: interiors — stars: rotation — Sun: rotation — turbulence

1. INTRODUCTION

Late-type rotating stars like the Sun possess convective envelopes in which highly turbulent motions are responsible for transporting heat, for redistributing angular momentum, and for building and dispersing magnetic fields. Theoretical descriptions for such turbulence pose fundamental difficulties, the greatest of which is that the active dynamical scales of motion span very many decades. This paper, the second in a series, utilizes direct numerical simulations of three-dimensional compressible convection to study a localized region in a rotating star, trading off overall domain size for sufficient spatial resolution to describe turbulent flows with some fidelity. The approach adopted here, as discussed in detail in Paper I of this series (Brummell, Hurlburt, & Toomre 1996; hereafter Paper I), deals with a Cartesian planar subdomain of a true spherical shell using a local modified *f*-plane model, as shown in Figure 1. Further, the physics is simplified as much as possible by dealing with a perfect gas, thereby seeking to understand the most basic dynamical effects of compressibility and rotation on the turbulent convection.

Paper I examined the differences in flow structure and evolution between laminar and turbulent compressible convection as the rotational influence was varied. It was found that rotating turbulent convection, much like nonrotating cases, possesses a seemingly laminar, cellular surface network that overlies a fully turbulent deeper interior (see Figs. 2, 6, and 7 in Paper I). The network consists of broad,

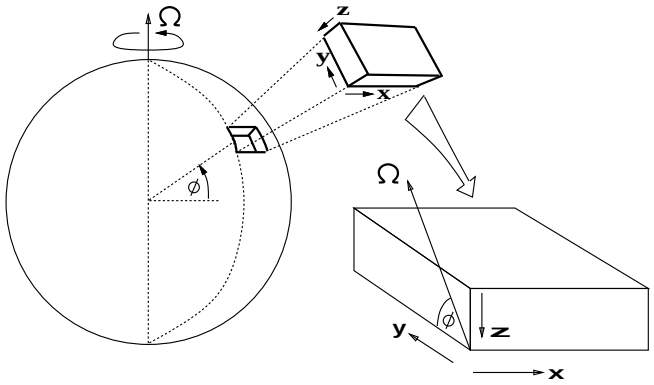

FIG. 1.—Local *f*-plane model positioned at latitude, ϕ, used to study flows in a portion of a spherical shell rotating with angular velocity Ω_0. The rectilinear coordinate system has the horizontal variables x increasing eastward and y poleward, the depth z increasing downward; the tilted rotation vector, $\mathbf{\Omega}$, thus lies in the y-z plane.

warm upflowing regions separated by narrow downflow lanes of cooler fluid joined in an irregular polygonal pattern. The presence of inertial oscillations associated with rotation contributes to considerable mobility in that network. The deeper turbulent region contains vortex tubes of many scales and orientations, including some distinctive large-scale coherent structures of vortical downflow that span the full vertical extent of the layer. The presence of such coherent and persistent structures amidst the intense turbulence of the interior and their tendency to align with the rotation vector, which at most latitudes is tilted from the local vertical, were the principal findings of Paper I. Such coherent structures yield crucial correlations between vertical and horizontal motions that generate mean Reynolds stresses and drive mean zonal (east-west) and meridional (north-south) flows, which are interpretable in turn as differential rotation and meridional circulations.

It is the object of this paper to study the resulting mean flows in some detail as the imposed parameters determining the vigor of the convective turbulence and the rotational influence are varied. Of particular interest is whether some contact can be made between the classes of mean zonal flows resulting from highly turbulent convection in these local models and the differential rotation profiles, with depth and latitude within the solar convection zone being deduced from helioseismology (see review by Gough & Toomre 1991). Such observations of the acoustic *p*-mode oscillations of the Sun have shown that the rotation profiles, obtained by inversion of frequency splittings of those modes (Libbrecht 1989; Brown et al. 1989; Tomczyk, Schou, & Thompson 1995; Thompson et al. 1996), are notably different from earlier predictions based on full spherical shell simulations of solar convection (e.g., Gilman & Miller 1986; Glatzmaier 1987). The convection in such global numerical simulations of rotating convection is dominated by columnar cells oriented in the north-south direction, whose tilting yields Reynolds stress terms that drive the zonal flows and thus form the differential rotation. These convection models predicted a zonal velocity profile that held the angular velocity nearly constant along the axes of the columnar cells and thus nearly constant on cylinders aligned with the rotation axis, decreasing with depth in the equatorial plane. Helioseismology suggests that the Sun operates differently, for its angular velocity at high latitudes in the convection zone appears to increase with depth, at midlatitudes is nearly constant on radial lines, and near the equator first increases and then slowly decreases with depth. At the base of the convection zone, such latitudinally varying angular velocity joins to the apparent solid body rotation of the deeper radiative interior via a strongly sheared adjustment layer. The recent advent of nearly continuous, full-disk imaged Doppler observation of solar oscillations from both the ground-based Global Oscillations Network Group (GONG) project and from the Michelson Doppler Imager (SOI-MDI) instrument on the *SOHO* spacecraft should enable more detailed assessment of large-scale mean flows within the Sun that can both inspire and challenge our understanding of turbulent dynamics deep within a star (Gough et al. 1996).

There is currently no resolution of the striking differences between the solar differential rotation profiles deduced from helioseismology and those obtained from theoretical models. Since helioseismic measurements are constantly improving, this paper seeks to address deficiencies in the previous numerical models. A plausible explanation for the discrepancies is that the spatial resolution available for the computation of rotating convection in full shells confined the simulations to laminar or mildly turbulent flows. Fully developed turbulence at Reynolds numbers, R_e, of order 10^{12} as estimated for the Sun may well redistribute angular momentum quite differently, thereby yielding other classes of mean flows and rotation profiles (see Brummell, Cattaneo, & Toomre 1995). Recent convection experiments (Heslot, Castaing, & Libchaber 1987; Castaing et al. 1989) and computations (DeLuca et al. 1990; Werne et al. 1991; Werne 1993), including some on compressible convection (Cattaneo et al. 1991), have shown that different regimes of turbulence can exist with subtly varying heat transport properties. These are often associated with the surprising degree of structure that may be embedded in otherwise chaotic flow fields (see also She, Jackson, & Orszag 1990; Vincent & Meneguzzi 1991; Porter, Pouquet, & Woodward 1994), arising from self-organizing processes (inverse cascades). Turbulent compressible convection, with symmetry broken by both rotation and stratification, appears to behave likewise, as exhibited in Paper I with the emergence of coherent structures once the flows become sufficiently turbulent. A novel turbulent transport mechanism for angular momentum, much like those responsible for new forms of heat transport, has the potential to resolve the solar differential rotation puzzle.

This paper focuses on analyzing the properties of the mean zonal and meridional shearing flows that can be induced by effects of rotation on turbulent compressible convection. Paper I explained in some detail the motivation for such simulations of rotating convection in localized domains, and thus § 2 restates the formulation only briefly. After reviewing the general properties of turbulent convection, § 3 in turn discusses the time dependence of the mean flows that are realized, their behavior as the degree of turbulence or the rotational influence is modified, and then assesses how the topology and structure of the convection yields the Reynolds stresses essential for both the generation and maintenance of the mean flows, finally examining the spiralling of the mean flows with depth and the mean helicity that is realized. Section 4 discusses the implication of these mean flows upon the deductions being drawn from helioseismology concerning the overall dynamics of the solar convection.

2. FORMULATION

The model used here for compressible convection in a rotating plane layer involves a rectilinear domain containing a fully compressible but ideal gas confined between two horizontal, impenetrable, stress-free boundaries a distance d apart. The upper surface is held at a fixed temperature, T_0, whereas a constant temperature gradient, Δ, is maintained at the lower boundary. The flow is assumed to be periodic in the two horizontal directions. The specific heats, c_p and c_v, shear viscosity, μ, thermal conductivity, K, and gravitational acceleration, g, are assumed constant. In hydrostatic balance, the temperature, T_p, density, ρ_p, and pressure, p_p, can exist in a polytropic state,

$$T_p/T_0 = (1 + \theta\tilde{z}/d) , \tag{1a}$$

$$\rho_p/\rho_0 = (1 + \theta\tilde{z}/d)^m , \tag{1b}$$

$$p_p/p_0 = (1 + \theta\tilde{z}/d)^{m+1} , \tag{1c}$$

for the vertical coordinate $0 \le \tilde{z} \le d$, where ρ_0 is the density at the upper boundary, $p_0 = (c_p - c_v)T_0\rho_0$, $m = -1 + g/\Delta(c_p - c_v)$ is the polytropic index, and $\theta = d\Delta/T_0$. The equations for the conservation of mass, momentum, and energy and the equation of state for a perfect gas can be nondimensionalized using d as the unit of length, the isothermal sound crossing time $[d^2/(c_p - c_v)T_0]^{1/2}$ as the unit of time, and T_0 and ρ_0 as the units of temperature and density, to produce

$$\partial_t \rho + \nabla \cdot \rho\boldsymbol{u} = 0 , \tag{2a}$$

$$\partial_t \rho\boldsymbol{u} + \nabla \cdot \rho\boldsymbol{u}\boldsymbol{u} + C_k P_r T_{a0}^{1/2}(\hat{\boldsymbol{\Omega}} \times \rho\boldsymbol{u}) = -\nabla p + P_r C_k[\nabla^2\boldsymbol{u} + \tfrac{1}{3}\nabla(\nabla \cdot \boldsymbol{u})] + \theta(m+1)\rho\hat{\boldsymbol{z}} , \tag{2b}$$

$$\partial_t T + \boldsymbol{u} \cdot \nabla T + (\gamma - 1)T\nabla \cdot \boldsymbol{u} = \frac{\gamma C_k}{\rho}\nabla^2 T + V_\mu , \tag{2c}$$

$$p = \rho T . \tag{2d}$$

Here $\boldsymbol{u} = (u, v, w)$ is the velocity, T, ρ, and p are the temperature, density, and pressure, respectively, and $V_\mu = [(\gamma - 1)C_k/\rho]P_r\,\partial_i u_j(\partial_i u_j + \partial_j u_i - \frac{2}{3}\nabla \cdot \boldsymbol{u}\delta_{ij})$ is the rate of viscous heating. Rotation enters the momentum equation in a modified f-plane formulation in this local model via the rotation vector,

$$\boldsymbol{\Omega} = \Omega_0\hat{\boldsymbol{\Omega}} = (\Omega_x, \Omega_y, \Omega_z) = (0, \Omega_0 \cos\phi, -\Omega_0 \sin\phi) , \tag{3}$$

where ϕ is the latitudinal positioning of the planar domain on the sphere, as illustrated in Figure 1. The rotation sense here has been changed for ease of comparison with the solar case since, in the z-downward coordinate system, positive rotation is clockwise when viewed from above the north pole. This paper adopts the more familiar counterclockwise rotation sense by setting $\Omega_0 \to -\Omega_0$ (equivalently $u \to -u$, $x \to -x$) when exhibiting the results.

The dimensionless numbers parameterizing the problem are the Rayleigh number,

$$R_a(z) = \frac{\theta^2(m+1)}{P_r C_k^2}\left[1 - \frac{(m+1)(\gamma-1)}{\gamma}\right](1 + \theta z)^{2m-1} , \tag{4}$$

involving the thermal dissipation parameter, $C_k = K/\{d\rho_0 c_p[(c_p - c_v)T_0]^{1/2}\}$ (the ratio of the sound crossing time to the thermal relaxation time), and $\gamma = c_p/c_v$ (the ratio of the specific heats), together with the Prandtl number, $P_r = \mu c_p/K$ (the ratio of the diffusivities of heat and momentum), and the Taylor number,

$$T_{a_0} = \frac{4\Omega_0^2 d^4}{(\mu/\rho_0)^2} = \left(\frac{\rho}{\rho_0}\right)^2 T_a . \tag{5}$$

Here R_a and T_a (the more usual Taylor number) are quoted as evaluated at midlayer in the initial polytrope.

A measure of the influence of the rotation on global motions derived in terms of these parameters is the convective Rossby number,

$$R_o = \left(\frac{R_a}{T_a P_r}\right)^{1/2} . \tag{6}$$

A value of R_o less than unity implies a significant influence of the rotation, since then in the time a fluid element is driven across the layer by buoyancy it can execute more than one inertial rotation. A true Rossby number, R_{o_t}, may be determined as the ratio of the root mean square (rms) vorticity generated in the convection to that of the rotating frame, i.e.,

$$R_{o_t} = \omega_{\rm rms}/2\Omega_0 . \tag{7}$$

It is found here that R_o and R_{o_t} are generally comparable.

At the upper and lower boundaries, it is required that

$$\rho w = \partial_z u = \partial_z v = 0 \text{ at } z = 0, 1 , \tag{8a}$$

$$T = 1 \text{ at } z = 0 , \quad \partial_z T = \theta \text{ at } z = 1 , \tag{8b}$$

which ensures that the mass flux and mechanical energy flux vanish on the boundaries. The total mass in the computational domain is conserved, and the imposed heat flux is the only flux of energy into and out of the system.

Averaging the momentum equations (eq. [2a]–[2d]) over the two periodic horizontal directions, x and y, produces the equations for the mean zonal (east-west) and meridional (north-south) flows:

$$\partial_t \overline{\rho u} = -\partial_z \overline{\rho u w} - f_z \overline{\rho v} + P_r C_k \partial_z^2 \bar{u} , \tag{9a}$$

$$\partial_t \overline{\rho v} = -\partial_z \overline{\rho v w} + f_z \overline{\rho u} + P_r C_k \partial_z^2 \bar{v} . \tag{9b}$$

Here, an overbar denotes the horizontal average and $f_z = P_r C_k T_{a0}^{1/2} \sin\phi$ is the inertial frequency for horizontal motions.

Equations (2a)–(2d) are solved numerically as an initial value problem by a semi-implicit, hybrid finite-difference/pseudospectral scheme. Spatially, the vertical discretization is by fourth-order finite differences, while the horizontal directions are represented by a Fourier collocation method. The time discretization utilized an explicit, two-level Adams-Bashforth scheme for all terms apart from the thermal conduction, for which a Crank-Nicholson scheme is used to avoid restrictive time stepping.

3. RESULTS

As summarized in Table 1, a series of runs has been made in the (R_a, T_a, P_r, ϕ) parameter space of the local model. All simulations were computed with an aspect ratio of 4:4:1, with $\gamma = 5/3$, and with an initial density contrast of $\chi_\rho = 11$ corresponding to a polytrope with $\theta = 10$ and $m = 1$. The layer then spans roughly five pressure scale heights initially, relaxing to a typical value of $\chi_\rho \sim 20$ as time progresses. The Rayleigh number is varied by altering C_k (effectively changing the fluid) while keeping P_r small so that the code

TABLE 1

PARAMETERS FOR THE f-PLANE ROTATING CONVECTION SIMULATIONS

Case	R_a	T_a	P_r	ϕ	(n_x, n_y, n_z)	R_o	$(R_a - R_{a_c})/R_{a_c}$	R_{e_λ}	$R_{e_{\rm rms}}$	$R_{e_{\rm max}}$	$\overline{E_k}/E_k$ (%)
L1.....	5×10^4	3×10^4	$10^{-1/2}$	45	$64 \times 64 \times 32$	2.29	9.23	3.06	141	372	2.13
L2.....	5×10^4	3×10^4	$10^{-1/2}$	90	$64 \times 64 \times 32$	2.29	2.78	2.40	120	318	0.40
L3.....	5×10^4	3×10^4	$10^{-1/2}$	15	$64 \times 64 \times 32$	2.29	21.5	4.36	169	377	8.63
R0.....	5×10^5	0	0.1	0	$192 \times 192 \times 130$	∞	420	14.03	925	2913	0
R1.....	5×10^5	10^5	0.1	45	$96 \times 96 \times 64$	7.07	182	12.85	932	2972	2.90
R2.....	5×10^5	10^6	0.1	45	$96 \times 96 \times 64$	2.24	111	8.72	764	2451	1.29
R3.....	10^7	5×10^7	0.1	45	$256 \times 256 \times 129$	1.41	109	11.33	2068	7621	0.46
R4.....	5×10^5	10^7	0.1	45	$96 \times 96 \times 64$	0.71	29.2	7.49	609	2068	0.68
R5.....	5×10^5	10^7	0.1	15	$96 \times 96 \times 64$	0.71	52.9	4.01	784	2383	3.72
R6.....	5×10^5	10^7	0.1	75	$96 \times 96 \times 64$	0.71	18.0	3.30	675	2053	3.90
T1.....	5×10^6	10^7	0.1	45	$192 \times 192 \times 96$	2.24	292	11.45	1703	5828	0.76
T2.....	10^7	2×10^7	0.1	45	$256 \times 256 \times 130$	2.24	378	11.83	2149	8108	0.79

operates in the regime where shear instabilities and vortex stretching are emphasized. The degree of instability, as measured by the departure of the Rayleigh number from the linear critical value, $R_a - R_{a_c}$, is shown in Table 1.

The degree of turbulence achieved in the resulting solutions is indicated by a Reynolds number, which measures the relative balance between advective and diffusive processes:

$$R_e(z) = \frac{U(z)\bar{\rho}(z)\ell}{C_k P_r}, \tag{10}$$

where ℓ and $U(z)$ are a typical length and velocity, respectively. There is not a unique choice for these typical values. The length scale may be chosen as the depth of the domain, and a typical velocity may be evaluated as the (time-averaged) rms velocity, $U_{\rm rms}$, or as the maximum velocity attained in the box, $U_{\rm max}$. Table 1 shows values of $R_{e_{\rm rms}}$ and $R_{e_{\rm max}}$ for these two choices, respectively. It is also useful to provide a Reynolds number, R_{e_λ}, based on the Taylor microscale, λ, and $U_{\rm rms}$. The Taylor microscale, defined as

$$\lambda^{-2}(z) = \overline{V_\mu}(z)/U_{\rm rms}(z), \tag{11}$$

represents the scale of dissipation associated with the rms velocity rather than the scale of the domain. These measures still indirectly include an indication of the stabilizing effect of rotation: increased rotational influence (for fixed R_a) decreases the scales of the fluid motion and therefore decreases any Reynolds number. Values of R_{e_λ} greater than about 10, or $R_{e_{\rm rms}}$ and $R_{e_{\rm max}}$ of about 10^3 or greater, indicate solutions that are at least moderately turbulent.

The solutions described in Table 1 are divided into three categories, which are denoted by a prefix of either L, R, or T. Cases labeled L are laminar, whereas all other cases are turbulent to varying degrees. Cases labeled T are the most vigorously turbulent cases. Cases R0–R4 are a series of solutions in which the rotational influence (as measured by R_o) increases for a fixed latitude, whereas cases R4–R6 maintain a strong rotational influence while varying ϕ.

3.1. *Nature of Turbulent Rotating Convection*

As discussed in Paper I, these simulations of f-plane convection draw on earlier nonrotating three-dimensional studies working with perfect gases (see, e.g., Cattaneo et al. 1991; Bogdan, Cattaneo, & Malagoli 1994). Increasing the degree of turbulence results in a striking transition from laminar overturning flow throughout the domain to a state in which the upper surface remains as a connected network of downflows surrounding broad upflows, yet disguising highly turbulent flows below. The convective flows near the upper surface, as in the perspective view of vertical velocities in Figure 2 (Plate 48), consist of a cellular network atop a fully turbulent interior, punctuated by vertically coherent structures emanating from the upper surface. The turbulent domain consists of fast, small-scale, nearly isotropic motions; the nearly laminar flow in the surface region is a consequence of the expansion of fluid elements rising through a rapidly decreasing density stratification near the top. Powerful downflows occur at the interstices of the upper network. These downflows pierce the interior turbulence, spanning the multiple scale heights from the top to the bottom of the domain. Despite being mobile, especially in the rotating case, these strong downflowing structures are spatially and temporally coherent, coexisting with the interior turbulence for many turnover times. The turbulent but structured nature of the flow is seen clearly in a volume rendering of enstrophy (vorticity squared) shown in Figure 2. The coherent downflows are strong, sizeable vortices that emanate from vorticity concentrated at the interstices of the upper network and punctuate the interior, where they are buffeted by much smaller, randomly orientated vortex tubes. The presence of such multiple scales is also revealed in horizontal planar rendering of both enstrophy and temperature fluctuations near the top of the layer, where the appearance is more ordered, and near the bottom, where the broad downflow systems are laced with intense vortex filaments (see Fig. 3 in Paper I and Figs. 4 and 5 in Brummell et al. 1995).

Coriolis forces change the nature of both the surface network and the turbulent interior in such convection. With the inclusion of rotational constraints, the scales of motion throughout are reduced, and the surface network becomes more curvaceous, less connected, and more time dependent. The overall mobility of the cellular pattern is due to inertial motions of the surface flows induced by the Coriolis forces. Spin-up of plumes under the rotational influence forces all downflows to be cyclonic and leads to increased vertical vorticity, often to the extent that an ensuing evacuation of the downflow vortex leads to buoyancy reversal and self-destruction of the structure, providing a new method for cell creation. More importantly, Paper I reveals that tilted flow structure (involving nonvertical cellular boundaries, streamlines, and coherent structures) can be readily achieved in compressible convection under the influence of rotation. When the flow is turbulent, the small-scale, fast-

overturning interior motions are more nearly isotropic and decorrelate from the inertial influence, leaving only structures with significant spatial and temporal coherence to sense the rotation. The strong vortical coherent plumes thus tend to form naturally in alignment with the tilted rotation vector.

Given such general properties of turbulent convection studied in Paper I, the main aim of this paper is to examine the persistent zonal and meridional mean flows that are produced by the interaction of rotation with the compressible convection. By definition, zonal motions are in the x-direction (east-west) and meridional motions are in the y-direction (north-south). Averaging the horizontal velocity fields, $u(x, y, z, t)$ and $v(x, y, z, t)$, found at any typical time, t, in each horizontal direction produces the mean zonal, $\bar{u}(z, t)$, and meridional, $\bar{v}(z, t)$, flows. The vector sum of these flows is an overall mean flow, $\bar{U}(z, t)$, at that time. Averaging over a long period in the simulation reveals the persistent vector mean flow, $\langle U \rangle$, made up of components $\langle u \rangle$ and $\langle v \rangle$ that are functions of z alone. Here, an overbar denotes an average over the horizontal directions x and y, and angle brackets imply a further averaging over time. The flows $\langle u \rangle$ and $\langle v \rangle$ represent the typical steady horizontal drift velocities at any depth. They are the local model equivalents of the zonal and meridional motions at the current latitude, ϕ, in the full spherical fluid shell and exhibit the differential motion with depth (equivalent to radius) at that latitude. By further examining a range of ϕ, they can also suggest the variation of such flows with latitude.

Figure 3 shows an example of the mean flows from case R4, with $\langle u \rangle$ and $\langle v \rangle$ shown as solid lines. Horizontal bars indicate the rms variation, and dotted lines indicate the peak variation of the mean velocities for the duration of the time averaging. In this solution, the zonal flow is primarily prograde (in the same sense as the rotation) with intervals of retrograde flow near the boundaries. The meridional flow is equatorward at the surface and poleward at the bottom but reverses away from the boundaries. In the absence of rotation, even though the equations permit mean flows, none have been realized in these simulations. With $\Omega = 0$, the creation of mean motions would require an internally generated spontaneous (reflectional) symmetry breaking by a mechanism like that of Howard & Krishnamurti (1986), for example. With the rotating f-plane model positioned away from the pole ($\phi \neq 90°$), the symmetry of the flow is automatically broken, and any solution must have definite handedness. All of the rotating solutions presented here therefore possess mean zonal and meridional flows, of which Figure 3 is an example. The mean flows are significant, although not dominant over the convection. Indeed, the percentage of kinetic energy contained in the mean flows, $\overline{E_k}$, as compared to the total kinetic energy, E_k, is less than 10% and typically only a few percent for the cases studied here (see Table 1). The properties of the mean flows, however, vary strongly with the degree of turbulence, the rotational influence, and the latitudinal positioning of the f-plane model.

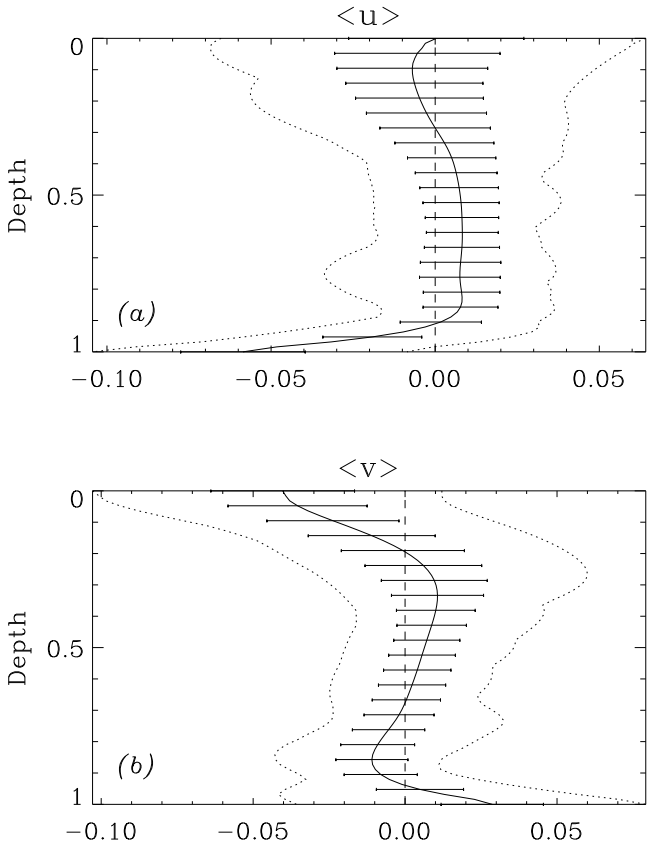

FIG. 3.—The horizontal- and time-averaged (*a*) zonal and (*b*) meridional mean flows, $\langle u(z) \rangle$ and $\langle v(z) \rangle$ respectively, for the simulation R4. The horizontal bars show the rms variation of the mean over the time of averaging for certain depths, and the dotted line shows the maximum and minimum values of that variation.

3.2. *Time Dependence of Mean Flows*

Many of the cases studied here possess a Rossby number, R_o, of order unity for which Coriolis and convective effects are of comparable importance. In this intermediate regime, inertial oscillations may be expected (e.g., Batchelor 1967; Pedlosky 1979). If an area of fluid diverges, it acquires a tangential acceleration (perpendicular to the radial expansion and the rotation vector) from the Coriolis force, forming an anticyclonic vortex. The resulting circular acceleration produces its own local centripetal force, which will tend in turn to contract the vortex. The interaction of the expansion and contraction produces an oscillation with frequency equal to that of the imposed rotation. For horizontal motions, this inertial frequency about the vertical is $f_z = 2\Omega_z = P_r C_k T_{a0}^{1/2} \sin \phi$. The mean flows here exhibit such oscillations, as seen in Figure 3 where they are largely responsible for the significant rms fluctuations and the large departures of the peak values from the time-averaged value. Figure 4 presents a clearer example of this time dependence of the mean flows. Phase plots of the mean zonal versus the mean meridional momenta are exhibited for three depths in the simulation T1, together with the corresponding time series and frequency spectra. The circular locii in the phase plots describe the inertial oscillations of the means, a signature that persists for all depths (although the temporal variation is smoother near the boundaries) and all solutions. In all cases studied, the measured spectra have a peak power close to that of the predicted inertial period, which for case T1 in Figure 4 is $\tau_i = 2\pi/f_z = 7.7$. The amplitude of the oscillations may be quite large compared to that of the underlying time-averaged mean flow (*solid squares* in the phase plots), possibly encompassing the origin so that the mean vector flow may reverse in time purely due to the inertial oscillations. Noting that such inertial time depen-

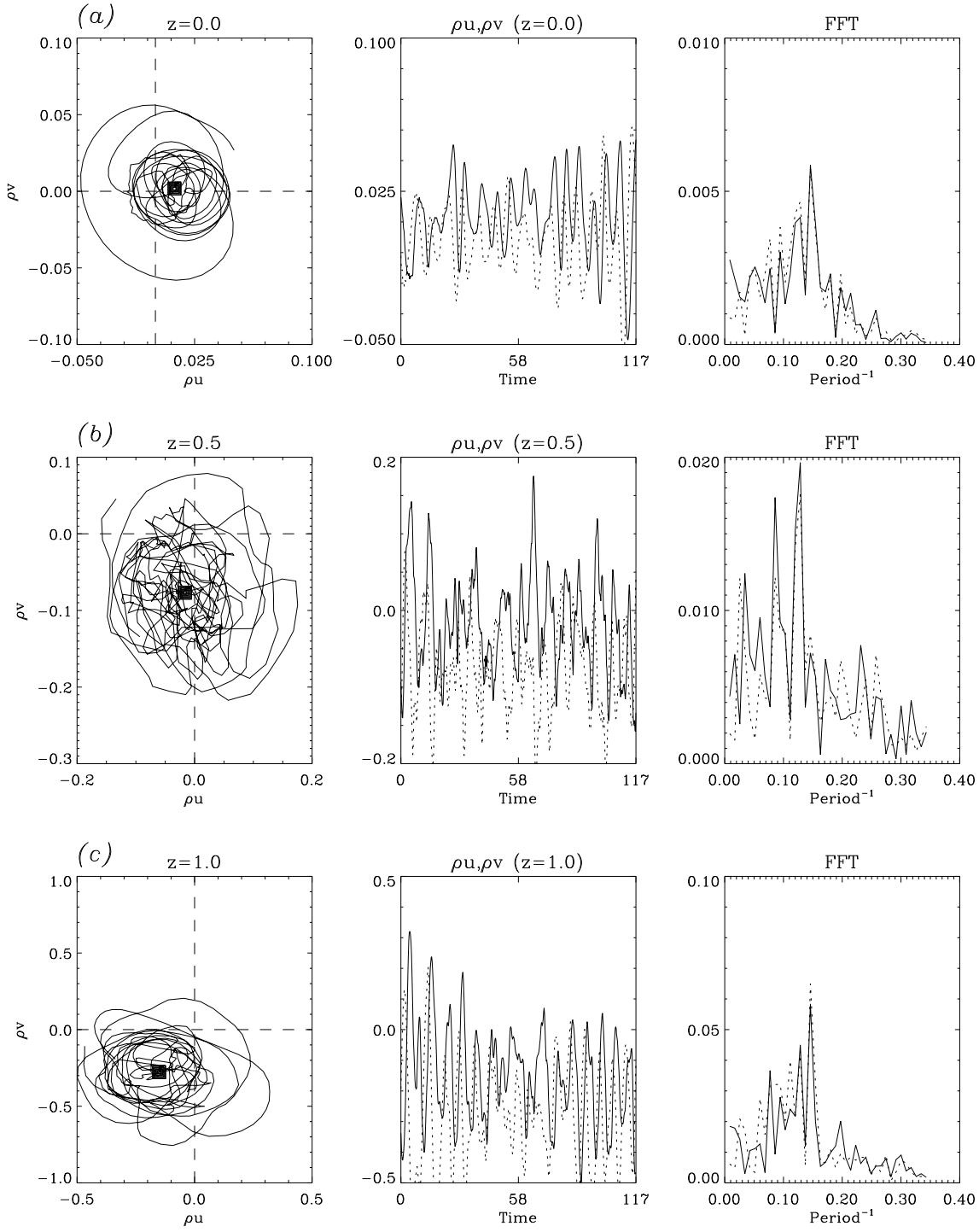

FIG. 4.—The rotational inertial oscillation in the time dependence of the mean flows in case T1. A phase plot of the mean momenta (ρu vs. ρv) is shown for three depths, (*a*) the top, (*b*) the middle and (*c*) the bottom of the domain, accompanied by the time sequence of those mean momenta and the spectrum of the frequencies in that time slice (ρu, *solid lines*; ρv, *dotted lines*).

dence is a prominent part of the resulting mean flows, the remainder of this paper concentrates on unravelling the nature of the persistent mean flows, $\langle u(z) \rangle$ and $\langle v(z) \rangle$, formed by time-averaging the components over many inertial times, τ_i.

3.3. *Increasing the Degree of Turbulence*

The characteristics of the mean flows that result are affected by the degree of turbulence achieved by the convection (indicated by R_e), by the influence of rotation imposed (as measured by R_o), and by the latitudinal positioning of the model domain. The nature of the mean flows is first examined for solutions that retain a comparable rotational influence while the level of turbulence varies, via cases L1, R2, T1, and T2. The degree of turbulence in these simulations, measured after the fact by the Taylor microscale Reynolds number, R_{e_λ}, ranges from 3 (laminar) to 12 (moderately turbulent) in a global average over the whole

domain, corresponding to a range of about 140–2150 in the large-scale Reynolds number, $R_{e_{\rm rms}}$. This succession of cases is achieved by suitably altering R_a and T_a for fixed P_r (see Table 1) so as to increase the degree of supercriticality (and therefore the nonlinearity) while keeping their ratio roughly constant, thus fixing the value of the thermal Rossby number, R_o. For these cases, R_o remains around 2.24, which indicates a moderate rotational influence. The mean flows, $\langle u \rangle$ and $\langle v \rangle$, generated are shown against depth in Figure 5, accompanied by the local measure of turbulence, R_{e_λ}.

Before examining the differences between the various solutions in Figure 5, it should be noted that all of the mean flows exhibit a reversal in direction at a depth of around $z = 0.75$. This crossover point is a fairly stable feature for these simulations since they share the same imposed density stratification. Earlier two-dimensional simulations (Hurlburt, Toomre, & Massaguer 1984) showed that the density contrast, χ_ρ, imposes an asymmetry on laminar compressible motions, whereby the roll-cell centers are skewed toward the lower boundary. The cell centers appear to lie at the level of the center of mass of the mean stratification, i.e., that depth where there is as much mass above as below. Intuitively, an extension of the finite laminar roll to infinite width would imply that the crossover of the mean flows should also be related to this point. Indeed, on examining the mean density profiles for many of the solutions here, this seems to be the case. For example, the time-averaged mean density of simulation T1 contains as much mass above $z = 0.72$ as below. Although the means are, in some sense, still smooth laminar flows, it is of interest that these highly turbulent solutions still exhibit this simplified behavior. Integrating the (steady) mean flow equations (eqs. [9a]–[9b]) with stress-free boundary conditions reveals the constraint that there must be zero total horizontal mass flux in each direction,

$$\int_{z=0}^{z=1} \overline{\rho u}\, \partial z = \int_{z=0}^{z=1} \overline{\rho v}\, \partial z = 0 \,. \tag{12}$$

This forces the mass fluxes to be either trivially zero (no mean flow at all) or to possess at least one zero-crossing at some depth. For a zero-crossing to lie at the center of mass then requires a remarkably well-balanced (mean) velocity distribution.

In Figure 5, both the zonal and meridional mean flows decrease in absolute amplitude throughout most of the depth as the degree of supercriticality is increased via solutions L1, R2, T1, and T2. The meridional flows, $\langle v \rangle$, maintain the same shearing profile with depth with the increase in degree of nonlinearity, although their amplitude is reduced. The zonal flows, $\langle u \rangle$, are reduced from strong shear flows in the more laminar cases (L1 and R2) to profiles that have only small amplitude in the interior, with regions of strong shear near the boundaries at the highest degrees of forcing shown (T1 and T2). Away from the upper thermal boundary layer, these more turbulent solutions have the sense of $\langle u \rangle$ reversed from that in the laminar solutions. The production of zonal and meridional mean flows appears to differ at high degrees of nonlinearity, with the meridional motions retaining some laminar character, while the zonal motions switch to a novel response.

It is intriguing that cases T1 and T2 exhibit very similar properties. These cases are both highly turbulent and share the same convective Rossby number, R_o, yet differ by a factor of 2 in the actual values of R_a and T_a. The similarities of the mean flow properties are striking and thus encouraging, since they may suggest that a regime of rotating turbulence exists where these results may be robust. That is, these findings may hold for higher R_a, provided that the rotational influence, R_o, is kept the same by scaling T_a and P_r. In much of the following presentation, the results for case T2 are omitted for clarity of the figures.

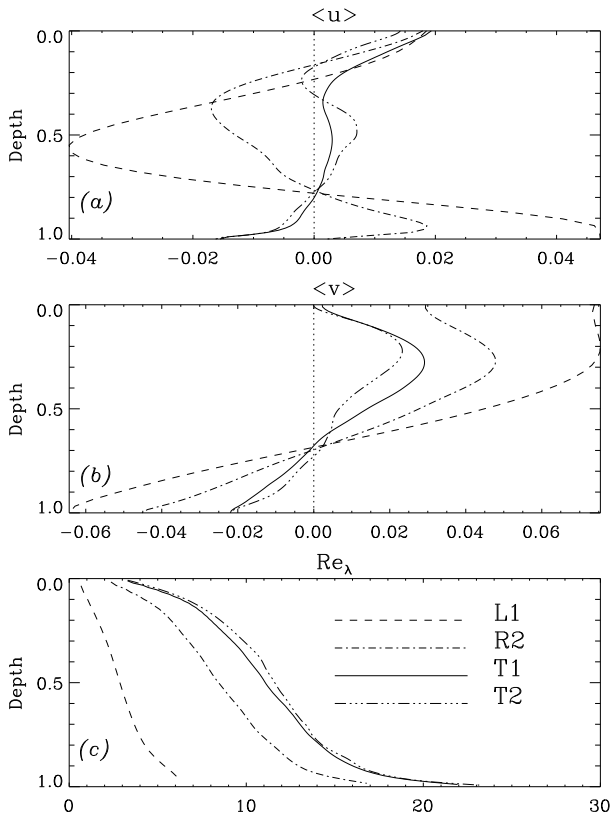

FIG. 5.—Plots of the mean velocity profiles, (*a*) $\langle u(z) \rangle$ and (*b*) $\langle v(z) \rangle$, in the zonal and meridional directions respectively, for simulations with a similar degree of rotation influence but varying degrees of turbulence (cases L1, R2, T1, and T2). The degree of nonlinearity is measured in terms of the Taylor microscale Reynolds number, which is also shown in (*c*) as a function of depth for each case.

3.4. *Increasing the Rotational Influence*

The effects of changing the rotational influence while maintaining an (approximately) fixed degree of nonlinearity is investigated next. Figure 6 shows plots of the mean zonal and meridional flows and the associated Taylor microscale Reynolds numbers as functions of depth for cases R0–R4. The thermal Rossby number ranges through the values $R_o = \infty$, 7.07, 2.24, 1.41, and 0.71 in these cases, which indicates an increase in the influence of rotation on the flow. Although the degree of supercriticality is not identical for all of these solutions, as is exhibited in the plot of R_{e_λ}, its variation is less than a factor of 2 for a range of parameters (T_a, R_a) that span (at least) 2 orders of magnitude. In particular, the values of R_{e_λ} are similar for cases R0, R1, and R3, as are those for cases R2 and R4, and so these cases may be fairly directly compared.

The nonrotating simulation case, R0, possesses no mean zonal or meridional flows. Mean flows are permitted in the absence of rotation, although the specific parameters chosen, such as the aspect ratio of the box, can influence

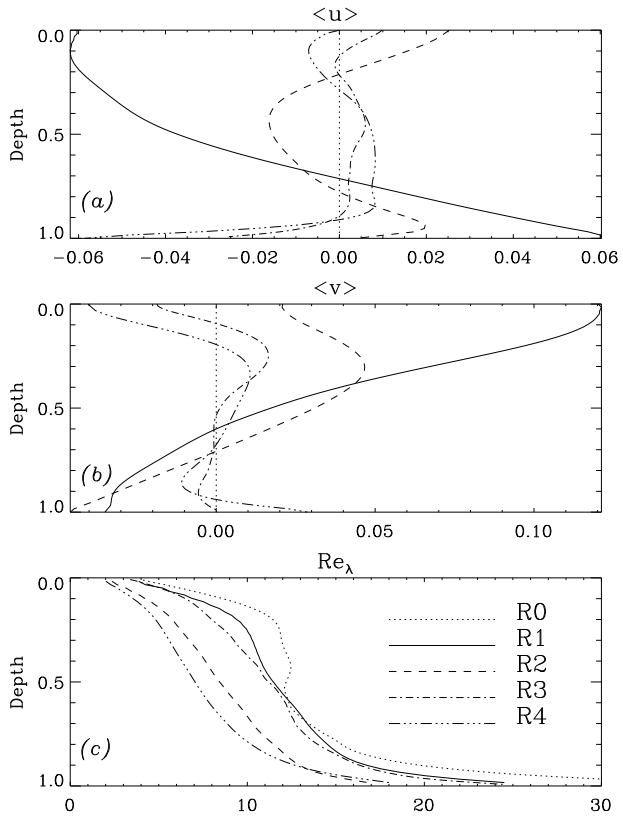

FIG. 6.—Plots of the mean velocity profiles, (*a*) $\langle u(z)\rangle$ and (*b*) $\langle v(z)\rangle$, in the zonal and meridional directions, respectively, for simulations with a similar degree of nonlinearity but varying degrees of rotational influence (cases R0–R4). The degree of nonlinearity is again exhibited in (*c*) as the Taylor microscale Reynolds number with depth for each case.

their production significantly (Rucklidge & Matthews 1993; Brummell & Julien 1997). The strongest mean flows in Figure 6 are achieved by the simulation R1 with $R_o \sim 7$. Strengthening the rotational influence in comparable solutions decreases the absolute amplitude of the mean flows. This decrease coupled with lack of mean flows for case R0 perhaps indicates that the strongest mean flows would occur at moderate Rossby numbers, $R_o > 7$. The general decrease in amplitude of the means may not be merely attributed to the stabilizing effect of increasing the Taylor number since, for example, cases R2 and R3 possess similar degrees of supercriticality and yet are included in the trend. The meridional mean flow, $\langle v\rangle$, maintains a simple linear shear profile in the interior as its amplitude decreases with decreasing R_o, joining strongly sheared reversals of the flow near the boundaries. Although $\langle u\rangle$ also exhibits a simple shear at the higher R_o of case R1, in the cases with lower Rossby numbers (R3, R4) the shear is considerably weakened to form a nearly constant profile in the interior accompanied, once again, by shear zones near the boundaries. The profile changes direction in the bulk of the interior as R_o decreases, as was found in the sequence of increasing degree of turbulence (Fig. 5). However, with a strong rotational influence, the constant interior profile is more pronounced, being significantly prograde.

3.5. *Varying the Latitude*

The solutions discussed previously were all calculated at midlatitude, $\phi = 45°$. The latitudinal positioning of the local domain can also have a substantial impact upon the development of mean flows. Figure 7 exhibits the resulting mean zonal and meridional velocity profiles for representative solutions at various latitudes. Figure 7*a* shows moderately rotationally influenced ($R_o = 2.29$) laminar cases at three latitudes, $\phi = 15°$, 45°, and 90° (cases L3, L1, and L2, respectively). Only weak mean flows are achieved when the domain is positioned near the (north) pole, with far stronger zonal and meridional means resulting at lower latitudes where the rotation vector becomes closer to the horizontal. In this laminar case, both mean flows are feeble (and indeed may vanish in a long enough time average) at $\phi = 90°$. Changing the latitude to $\phi = 45°$ increases the peak amplitude of both zonal and meridional means comparably, but a further shift to $\phi = 15°$ amplifies the zonal mean to a strong shear yet leaves the meridional flow roughly the same.

Figure 7*b* displays turbulent cases that are strongly rotationally influenced ($R_o = 0.71$) for latitudes $\phi = 15°$, 45°, and 75° (cases R5, R4, and R6, respectively). The zonal mean flows produced in these turbulent cases remain qualitatively similar in profile despite the varying latitude. Each zonal profile exhibits a nearly uniform interior extending over the range $0.4 < z < 0.8$, sandwiched between stronger boundary shear flows. The meridional mean flows consist mainly of boundary shear zones with a weak nonuniform interior. The amplitudes of all these means again increase with decreasing latitude, much as for the laminar cases.

3.6. *Generation of Mean Flows: Topology of the Convection*

The generation and maintenance of the zonal and meridional flows is governed by the mean flow equations (eqs. [9a]–[9b]). The first term on the right-hand side of each equation corresponds to a generation of the mean component through nonlinear interactions of the fluctuating velocities. These second-order correlations of the velocities are often referred to as the Reynolds stresses. The second terms in equations (9a) and (9b) represent a coupling between the mean horizontal motions by Coriolis forces, and the third terms correspond to viscous diffusion of the mean flows. The Reynolds stress terms are the only source terms in these equations. The vertical derivative of these stresses, modified by the action of the diffusive terms, determines the strength of the mean flows produced. The Coriolis terms serve only to swap energy between the two mean components and do no net work. In a steady state (or, equivalently, a long-term time average), equations (9a) and (9b) reduce to

$$f_z \overline{\rho v} = -\partial_z \overline{\rho u w} + P_r C_k \partial_z^2 \bar{u} \,, \tag{13a}$$

$$f_z \overline{\rho u} = \partial_z \overline{\rho v w} - P_r C_k \partial_z^2 \bar{v} \,. \tag{13b}$$

(Note that for comparison with the solar case, the results here are presented with $f_z < 0$, since Ω_0 has been replaced by $-\Omega_0$ or, equivalently, $u \to -u$). The simulations reveal that the diffusive terms in equations (13a) and (13b) are generally small and that the resulting persistent mean zonal and meridional flows are produced via a balance between the Coriolis and Reynolds stress terms. A strong correlation between u and w produces mean meridional momentum; a similar correlation between v and w produces mean zonal momentum. Clearly, any mechanism that introduces a net tilted flow into the system yields a correlation between vertical and horizontal momenta and therefore serves to generate mean flows. Thus the topology and structure of the

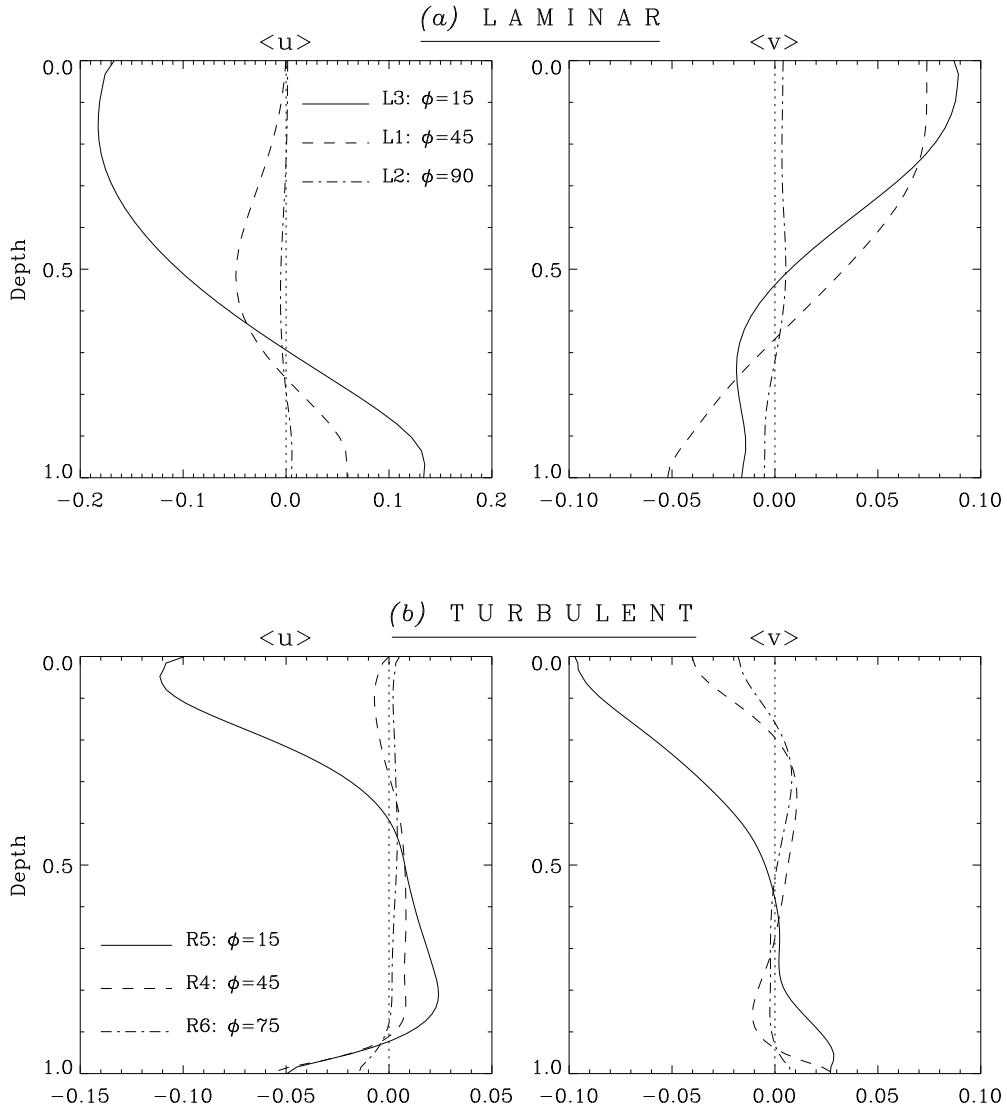

FIG. 7.—Time-averaged mean zonal ($\langle u \rangle$) and meridional ($\langle v \rangle$) velocity profiles with depth, for three latitudes, $\phi = 15°$, 45°, and 75°. (*a*) Cases with moderate rotational influence, $R_o = 2.29$, in a laminar regime (L1–L3). (*b*) Cases with strong rotational influence, $R_o = 0.71$, in a more turbulent regime (R4–R6).

convective flows are crucial ingredients in the understanding of the Reynolds stress terms and the associated mean flows.

Paper I showed that tilted flow structures related to nonvertical particle paths, cell boundaries, and other coherent structures are realized in compressible convection under the influence of rotation. However, the resulting correlated flows differ according to the circumstances. With the tilted rotation vector of the modified *f*-plane model utilized in these simulations, both horizontal and vertical components of $\mathbf{\Omega}$ are present. For laminar convection, the flows are cellular and the nonlinear production of vertical vorticity from the convectively driven horizontal vorticity is weak. Therefore, the action of the horizontal component of $\mathbf{\Omega}$ dominates, tilting cellular streamlines in the zonal direction. This provides a strong correlation between vertical and zonal motions, which produces a source for persistent meridional mean flows in the long-term time average.

When conditions are such that the convection is turbulent, the resulting flow structure is different. An example is shown in Figure 2. Turbulent compressible convection retains a cellular network of downflowing lanes surrounding broad upflowing regions near the upper boundary where the density stratification decreases rapidly. However, this laminarized region sits atop small-scale, horizontally isotropic turbulent motions deeper in the domain where the vorticity components are well mixed owing to the strong nonlinear interactions. This turbulent interior is punctuated by coherent structures, which are the strong vortical downflowing plumes emanating from the interstices of the upper network. The small-scale, fast-overturning interior motions decorrelate from the inertial influence. An overall reduction in the amplitude of the mean flows and the momentum transports with increasing degree of turbulence may then be anticipated. For laminar convection, strong means are generated by the action of rotation on the large-scale overturnings, producing bulk tilted streamlines and cellular boundaries (see discussions of rotating Boussinesq convection in Hathaway, Gilman, & Toomre 1979; Hathaway, Toomre, & Gilman 1980; and Hathaway & Somerville 1986). Increasing the Reynolds number decreases the scales of motion, reduces their turnover time, and decorrelates the

velocities. Such small-scale random eddies do not not sense the rotation since their lifetime is small compared to the rotation time, and therefore their effective Rossby number is high. This loss of coherence, due to the increase of turbulence and the decoupling of the motions from the rotation, substantially reduces the Reynolds stress correlations required to build the mean flows, and thus the overall amplitude of the means may be expected to decrease.

However, Paper I showed that a novel form of correlation can be induced when the fluid flow takes on its turbulent topology and the rotational influence is potentially strong. While small-scale interior motions decorrelate, structures with significant spatial and temporal coherence may still sense the rotation. The coherent structures that pierce the turbulent flow over multiple density scale heights tend to form naturally in alignment with the rotation vector. Since $\mathbf{\Omega}$ lies in the y-z plane in this model, such turbulent alignment encourages correlations between vertical and meridional velocity components and thus can generate Reynolds stresses that drive zonal mean flows in the long-term average. The turbulent alignment of coherent structures cannot contribute directly to steady meridional mean flows owing to the orientation of the rotation vector. One of the more intriguing results exhibited in these solutions is that although both meridional and zonal mean flows become reduced in amplitude in the turbulent cases, the zonal flow retains a weak but roughly constant profile with depth (at least away from the boundaries) as the convective Rossby number is decreased. Though there is a general decorrelation associated with the turbulent motions, an imprint of the rotationally aligned coherent structures remains, providing the dominant Reynolds stress contributions that drive the zonal flow profile.

Positioning the domains at higher latitudes may be expected to diminish both laminar and turbulent production of the mean flows because the y-component of $\mathbf{\Omega}$ decreases in amplitude as the domain is moved toward the pole. If the flow is laminar, then the tilting action of Ω_y on the streamlines and cellular boundaries is decreased. In the turbulent regime, as the rotation vector becomes more vertical, the aligned strong vortical structures become less tilted, and the resulting correlations between meridional and vertical velocities are reduced. Hence, positioning the f-plane domain nearer the pole weakens the source correlations for mean flows and thus reduces their amplitude while retaining the turbulent or laminar shape of the profile. At low latitudes, however, the laminar and turbulent mechanisms can both act to strengthen the mean flows, since the horizontal component of the rotation vector is now the dominant element. Strong laminar zonal tilting then provides enhanced uw correlations and meridional mean flows. Turbulent alignment here produces elongated coherent structures nearly parallel to the y-axis, providing stronger vw correlations and thus zonal mean flows. These results are reflected in Figure 7.

3.7. *Generation of Mean Flows: Reynolds Stresses*

Examination of the Reynolds stress sources for the generation and maintenance of mean motions in highly turbulent, compressible convection is clearly desirable but presents a number of challenges. The turbulent flows here are highly variable and intermittent, which makes correlations hard to isolate amidst the chaotic background. The coherent structures, which can provide some correlation, occupy only a small fraction of the whole domain, and thus their effects can easily be lost in any sizeable average. Such downflow structures also possess strong vertical vorticity, which provides a significant local correlation between the single-signed vertical motion and both senses of the horizontal motions. The small underlying drift correlation must be extracted from these nearly cancelling, large correlations by integration over particle trajectories. In addition, the flow is strongly time dependent, including the inertial oscillations encouraged by the rotation that exhibit large amplitude excursions compared to the overall persistent mean, as in Figure 4. All these effects accumulate to make instantaneous estimates of the Reynolds stress sources noisy and therefore relatively useless, and thus long-term time averages must be used.

Displaying the time-averaged source terms from equations (9a) and (9b) (the z-derivatives of the Reynolds stresses) supplies no new information, since they return precisely the mean momenta, suitably scaled and with a small error due to the diffusive term (as highlighted by eqs. [13a] and [13b]). Instead, Figure 8 presents the Reynolds stress correlations themselves time-averaged over many turnover and inertial times in some representative calculations. Both zonal, ρuw, and meridional, ρvw, Reynolds stresses are shown averaged horizontally and in time for the cases exhibiting varying degrees of turbulence and varying rotation (corresponding to Figs. 5 and 6). For relatively laminar (L1, R2) and weakly rotationally influenced (R1, R2) flows, there is a generic shape to the profiles. The stresses are zero at the boundaries and exhibit a smooth positive maximum in the interior. This reflects the amplitude variations of the fluctuating velocities with depth rather than a higher degree of correlation, since these values are not scaled by the amplitudes. The positive correlation is an indication of the dominant laminar tilting of streamlines and cellular structure, as explained in detail in Paper I. Increasing the degree of nonlinearity reduces the overall amplitudes owing to a general decorrelation of motions associated with the increasingly chaotic flow. However, for turbulent motions with moderate (T1) or strong (R3, R4) rotational influence, the profiles can change significantly, particularly in the resulting meridional stresses. Indeed, $\langle \rho vw \rangle$ changes sign from positive to negative in the interior in going from the relatively laminar simulations (L1, R2) to the more turbulent ones (T1) and also with the increasing influence of the rotation between the weakly (R1, R2) and strongly (R3, R4) influenced solutions. The associated zonal stresses, $\langle \rho uw \rangle$, in general remain positive in the interior. This change of sign in the meridional Reynolds stress (and the equivalent sign switch in the associated scaled correlations shown in Table 2 of Paper I) reflects the increased importance of the turbulent alignment of coherent vortical structures with increasing degree of turbulence and decreasing Rossby number. As such structures become aligned with the rotation vector, they provide more definite negative ρvw correlations between the downward motion of the plume and its tilt to the south. Although these structures are not very space-filling, their correlation appears to be felt in the meridional stresses. The subsequent change in sign with varying R_a and R_o leads to the corresponding reversal of the zonal mean flow seen in Figures 5 and 6. The mainly negative meridional stress profile for R4 has its minimum shifted to lower depths, and the relatively constant gradient leading down to this provides the z-independent interior for the

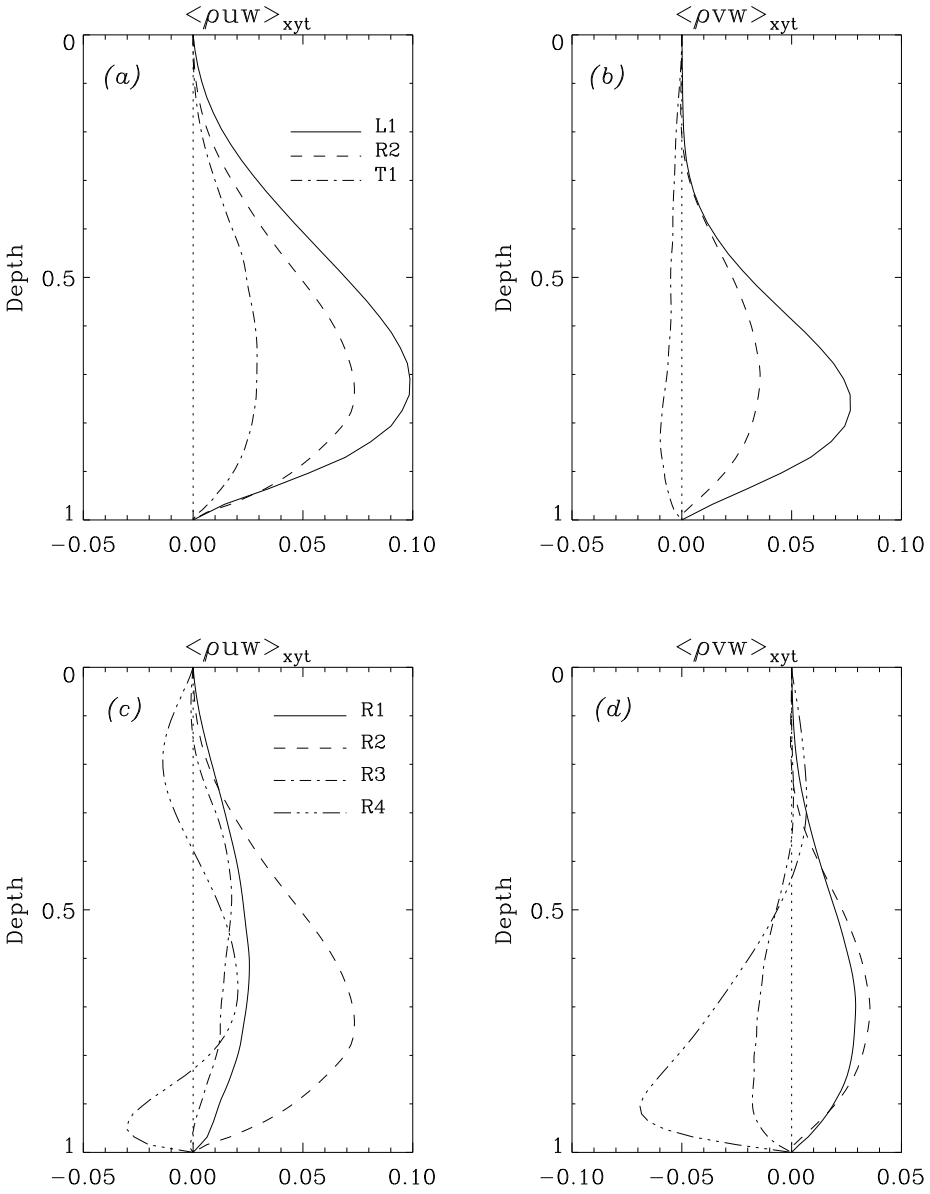

FIG. 8.—Time-averaged mean zonal ($\langle \rho uw \rangle$) and meridional ($\langle \rho vw \rangle$) Reynolds stresses against depth. Panels (*a*) and (*b*) show cases where the rotational influence is roughly constant and the degree of nonlinearity is varied, as in Fig. 5. Panels (*c*) and (*d*) show cases R1–R4 where the degree of turbulence is roughly the same but the rotational influence varies, as in Fig. 6.

zonal mean flow of this case. These low R_o, turbulent Reynolds stress profiles do not simply reflect the rms velocity profiles (as in the laminar cases), but rather exhibit the different degrees of velocity correlation.

The presence of mean horizontal motions implies that there is a net vertical transport of horizontal momenta, and this is exactly described by the Reynolds stresses shown in Figure 8. The stresses, ρuw and ρvw, can be considered as the vertical transports of zonal and meridional momenta, respectively, where a positive value indicates a net downward transport of positive momentum. Figure 8 then shows that in almost all cases there is a net downward transport of positive (eastward) zonal momentum. Zonal momentum is extracted from the upper layers and deposited in the lower layers, with the strength of this transport decreasing with increasing turbulence, owing to decorrelation of the motions. In contrast, the transport of positive (northward) meridional momentum switches from downward to upward as the degree of nonlinearity or the rotational influence is increased.

3.8. *Spiralling Mean Flows and Helicity*

These simulations also reveal that the direction of the total mean flow has a tendency to spiral with depth. Figure 9 exhibits the vector sum, $\langle U(z) \rangle$, of the mean flow components, $\langle u(z) \rangle$ and $\langle v(z) \rangle$, at each depth, shown in a three-dimensional format for the case T1 as an example of such behavior. An arrow is drawn at chosen depths, z_i, pointing in the direction of the vector sum, $\langle U(z_i) \rangle$, with its length proportional to the amplitude, $|\langle U(z_i) \rangle|$. The combined picture represents what would be seen if a stack of weather vanes were placed in the fluid, where the steady mean flows alone were operating. It is typical for at least part of this weather vane plot to align itself such that the arrows describe a spiral with depth. The sense of the spiralling in these simulations may be measured in terms of the angle

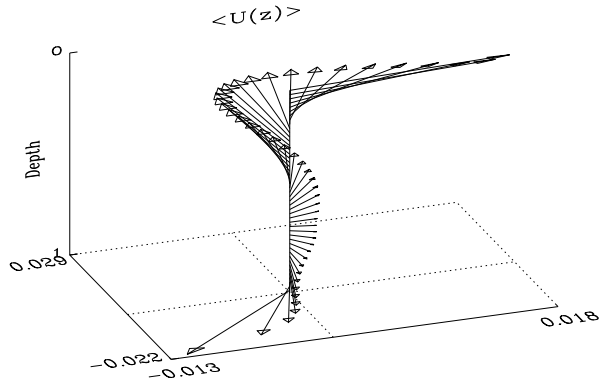

FIG. 9.—A vector plot with depth (colloquially referred to as a weather vane) of the time-averaged total mean flow velocity, $\langle U(z)\rangle$, for case T1, demonstrating the cyclonic and anticyclonic spiralling nature near the upper and lower boundaries respectively. Only a subset of the 96 available z_i depths are shown for clarity.

that the mean vector subtends with the x-axis as a function of depth,

$$\Phi_u(z) = \tan^{-1}\left[\langle v(z)\rangle / \langle u(z)\rangle\right], \tag{14}$$

and its derivative,

$$\partial_z \Phi_u(z) = \frac{\langle u(z)\rangle \partial_z \langle v(z)\rangle - \langle v(z)\rangle \partial_z \langle u(z)\rangle}{\left[\langle u(z)\rangle^2 + \langle v(z)\rangle^2\right]}. \tag{15}$$

Where the angle is increasing with depth ($\partial_z \Phi_u > 0$), the sense of the spiralling is cyclonic, and the vector arm swings in the direction of the rotation as depth increases. Where the angle decreases ($\partial_z \Phi_u < 0$), the spiral is anticyclonic.

Figure 10 plots the angle, Φ_u, with depth for some of the simulations, and some trends may be observed. In general, the mean vector spirals cyclonically (with increasing depth) near the upper boundary and reverses to spiral anticyclonically near the lower boundary. The spiralling is probably related to Eckman-like boundary processes, and thus the effect is more noticeable at the upper surface where the thermal boundary layer is thicker, owing to the stratification. The laminar cases (e.g., L1, L2, and L3) appear to spiral significantly throughout the whole layer, with the change from cyclonic to anticyclonic near the center of gravity of the layer. The turbulent cases (e.g., R2, R3, and T1) tend to consist of an interior of relatively small-amplitude, more disorganized mean flows connecting the two boundary layer spirals. Away from the boundary layers, if the flow is turbulent in the interior, the motions are generally enhanced toward isotropy by the rotation (see Paper I). The scales are small compared to the density scale height, and the motions turn over quickly compared to the inertial time, therefore sensing both the stratification and the rotation only weakly. The sense of the spiralling is therefore more random in the interior. However, some rapid swings of the mean velocity vector across angles, observable in Figure 10 as more horizontal portions of the curves, appear consistently in many of the simulations. This rapid spiralling is associated with the zeroes of the mean velocities. When the mean components become small, $(\langle u\rangle^2 + \langle v\rangle^2)$ decreases and the rate of spiralling, $\partial_z \Phi_u(z)$, increases. Physically, this spiralling is only rapid because the vector is close to the origin, so that small changes in $\langle u\rangle$ or $\langle v\rangle$ translate to large angular displacements. As discussed earlier, there is often a zero of both $\langle u\rangle$ and $\langle v\rangle$

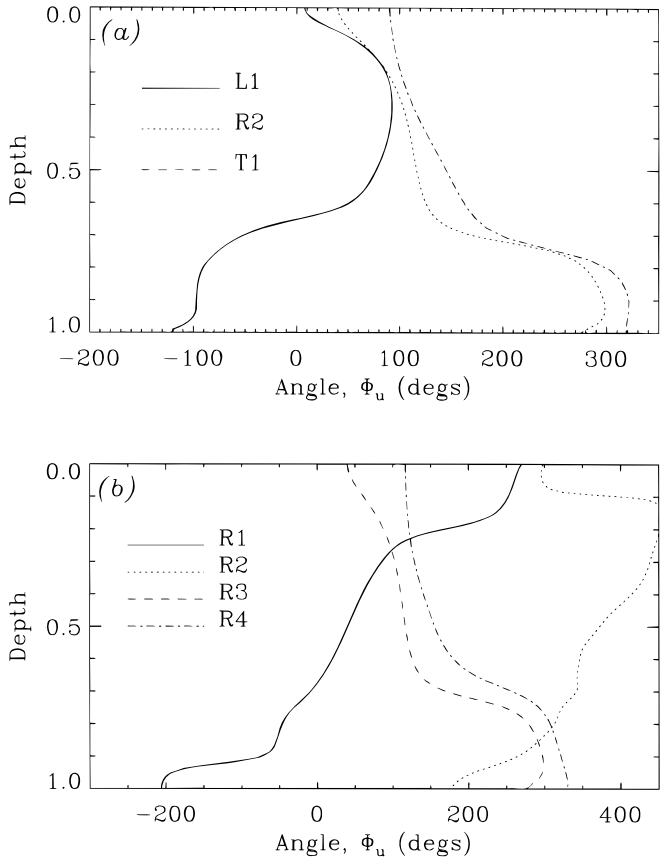

FIG. 10.—The sense of the spiralling of the mean flows. Plots of the variation of the angle, Φ_u, between the x-axis and the (time-averaged) vector mean flow direction, $\langle U(z)\rangle$. (*a*) Cases L1, R2, and T1, where the rotational influence is roughly constant but the nonlinearity increases. (*b*) Cases R1–R4, where the Reynolds numbers are similar, but the rotational influence increases (R_o decreases).

associated with the center of gravity of the cell at roughly $z = 0.75$ in many of the solutions shown, and the spiralling is sensitive to these points.

The spiralling of the mean vector exhibits a definite handedness that generally switches sign in the interior. This handedness suggests that the helicity of the flow may be of some interest. Figure 11 displays time and horizontal averages of the helicity, $H = \boldsymbol{u} \cdot (\nabla \times \boldsymbol{u})$, for the same simulations. Clearly, the mean helicity is generally positive in the upper regions and negative in the lower regions for all cases. Although this result concurs with the handedness of the mean spirals, the two are not directly related. The mean helicity is dominated by the vertical vorticity of vertical motions. The mean flow does indeed possess helicity, but this is constructed entirely out of horizontal vorticity, since the mean cannot possess vertical vorticity. Indeed, on examination, the mean flows contribute very little to the mean helicity, the majority arising from the fluctuating velocities.

The distinct mean helicity profiles shown are indications of the dominance of coherent structure (plume) dynamics within the overall flow. In the upper thermal boundary layer, a cellular downflow network is formed by the convergence of horizontal motions. Major coherent structures or plumes are created at the interstices of the network by further convergence of flows along the downflow lanes. The formation of such downflowing plumes by local con-

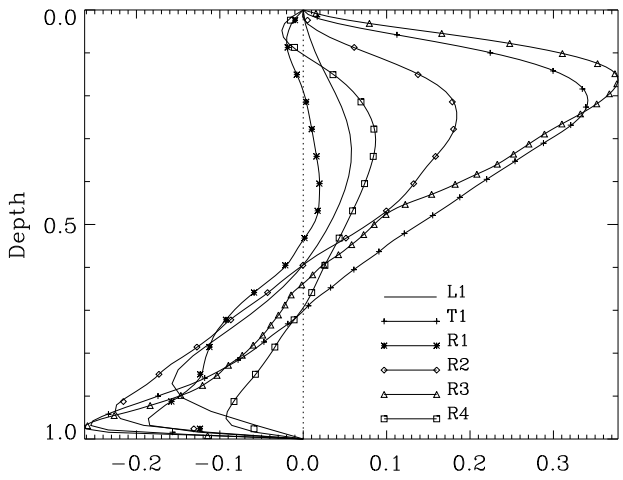

FIG. 11.—Mean helicity, $\overline{H} = \overline{\boldsymbol{u} \cdot (\nabla \times \boldsymbol{u})}$, as a function of depth for the cases L1, T1, and R1–R4. For this wide range of solutions, the mean helicity profile is generally positive in the upper portion of the layer and negative in the lower.

vergence of flows requires them to spin up under the background rotation in order to conserve angular momentum locally. Hence, all downflow structures near the upper boundary must be cyclonic. Since the total horizontal divergence (and similarly the total vertical vorticity) must be zero in any horizontal plane, the upflows must diverge and be anticyclonic. These effects enforce a positive helicity in the upper portions of the domain. If the simulations possessed a midplane reflection symmetry, as they would if the equations solved were Boussinesq (with symmetric boundary conditions), then an equal and opposite sign of helicity would be expected from equivalent process at the lower boundary. At the bottom, upward-directed plumes would be formed from locally converging horizontal flows and would spin up cyclonically. The opposite sense of helicity would result since the vertical motion has reversed, while the cyclonic vertical vorticity is retained. This is indeed observed in Boussinesq simulations (Julien et al. 1997). The equivalent effect at the lower boundary in the current simulations is similar, but it is diminished by the lack of midplane symmetry in the compressible equations under the imposed stratification (and nonsymmetric boundary conditions). The asymmetries retard plume ejection from the lower boundary in favor of downflow-dominated convection driven from the upper surface. Rising plumes are forced to expand under the imposed stratification counteracting their natural helicity, enhancing the positive surface helicity but undermining the negative helicity at the lower boundary. However, even in this scenario, the splashing and subsequent divergence of the strong downflow structures against the lower boundary enforces some upflow convergence, thus still providing a negative mean helicity at the bottom. The impenetrable boundary conditions in these simulations are convenient but artificial, and such lower boundary effects may change in the presence of more relaxed bottom boundary conditions, such as in studies of penetrative convection (Clune, Brummell, & Toomre 1997).

4. CONCLUSIONS

The localized *f*-plane domains of rotating compressible convection considered here and in Paper I have provided a means to obtain sufficient spatial resolution in the simulations to study fully turbulent flow regimes. Though such local models represent a major compromise compared to dealing with the full curved geometry of a rotating shell, they offer a route for examining the form of the mean zonal and meridional shearing flows that coexist with turbulent convection influenced by rotation. The approach here, which deals with a perfect gas and idealized boundary conditions, has sought to focus on the intrinsic dynamical properties of the coupling of turbulent convection with rotation. Certainly these studies have simplified the physics to the extreme, since effects of ionization, magnetic fields, radiative transfer, and variations of the fluid properties have all been ignored. Such processes could in due course be incorporated, though a higher priority has been to attain sufficiently turbulent flow conditions to assess the character of the associated mean flows and to elucidate possible turbulent momentum transport mechanisms that may lead to notable differences in the generation and maintenance of the mean flows. Though the recent helioseismic deductions pertaining to differential rotation deep within the solar convection zone have served as a major stimulus for these studies, it is clear that the Reynolds and Prandtl numbers accessible in present turbulence simulations are still many orders of magnitude away from the solar conditions (Brummell et al. 1995). These studies then have a primary role in helping to develop and refine our physical intuition about the nature of the mean flows that can coexist with turbulent convection, while recognizing that more turbulent states may well experience a somewhat different set of dynamical rules.

All of the cases of rotating compressible convection studied here possess mean flows in both the zonal and meridional directions. The amplitudes of the mean flows depend on the degree of nonlinearity of the convection (as measured by the Reynolds number) and the influence of rotation (as measured by the Rossby number), but in general contain on the order of a few percent of the total kinetic energy. Increasing the degree of nonlinearity in the simulations while retaining the same global rotational influence reduces the amplitude of the mean flows in the interior of the layer, where the scales of convection become smaller, more isotropic, and decorrelated with the increased degree of turbulence. When the rotational influence on turbulent solutions is significant, an alignment of coherent vortex structures with the axis of rotation (confined to the vertical-meridional plane) is observed, accompanied by modest prograde zonal mean flows in the interior. This turbulent zonal flow profile is distinct from the laminar and weakly rotationally influenced mean profiles. The laminar profiles are strong, substantially sheared, and produced from positive Reynolds stresses generated by the laminar tilting of streamlines and cellular boundaries. The turbulent mean flow profiles are weak owing to the chaotic decorrelation of the motions, yet when the rotational effects are strong enough, they can become dominated by the vertical-meridional interactions in the aligned vortical structures. The meridional Reynolds stress can change sign in accordance with these correlations, reversing the zonal flow to form a small-amplitude but constant prograde zonal mean across the interior of the layer. The interplay between the laminar streamline alignment, which can generate both zonal and meridional mean flows, and the turbulent structural alignment, which favors constant zonal flows, is quite delicate and dependent on the simulation parameters.

The nearly uniform zonal mean flow with depth realized in these simulations is intriguing, for it shares some of the features of the solar differential rotation profiles inferred from helioseismology (e.g., Thompson et al. 1996). The splitting of *p*-mode frequencies suggest a nearly constant angular velocity with depth over much of the convection zone. The angular velocity observed near the surface, where the rotation is faster at the equator than near the poles, prevails throughout the bulk of the convection zone with little radial dependence. This profile culminates in a region of strong shear at the base of the convection zone, known as the tachocline (e.g., Spiegel & Zahn 1992), where the variable angular velocity with latitude appears to adjust to nearly solid body rotation in the deeper radiative interior. There is also a thin boundary layer of shear near the surface, where the angular velocity increases with depth at low and intermediate latitudes. The simulations presented here can (for certain parameters) likewise possess a constant-with-depth zonal mean profile in the interior accompanied by prominent regions of shear near both the upper and lower boundaries. However, such shearing features deduced from these *f*-plane convection models must be viewed with caution, for the boundary regions in the model involve drastic simplifications. For example, near the top of the model domain, the effects of radiative transfer and ionization are ignored, and near the bottom, the flows are abruptly turned by an impenetrable, nondeformable boundary. New simulations are under way to relax the latter constraint somewhat by allowing penetration from the convecting layer into a lower stable layer of fluid (Clune et al. 1997), and it remains to be seen how the shear survives near the interface between the two layers. It is possible that the mean flows in the turbulent interior may be sufficiently decoupled from effects attributable to the precise boundary conditions to possess properties that are quite robust. Indeed, as well as the constant-with-depth profile in the bulk of the layer, the model also yields zonal flows that have greater prograde values at lower latitudes than at higher latitudes, as shown in Figure 7*b*, thus exhibiting equatorial acceleration with respect to the poles. In these simulations, this appears to be due to the presence of turbulent and laminar alignment mechanisms and whether they both act (at low latitudes) or are both absent (at high latitudes).

The *f*-plane simulations here are carried out at very modest Reynolds numbers as compared to those of the Sun, and this may explain some of the discrepancies between some aspects of the mean flows attained and those deduced from solar observations. The sense of the zonal flow at the surface found here (and in the calculations of Hathaway & Somerville 1986) is retrograde to the rotation, which is contrary to the observed solar result, although the interior of the layer is correctly prograde. Though this prograde interior exhibits a tendency toward an equatorial acceleration that concurs with the trend deduced from helioseismology, the bulk of the solar convection zone exhibits a considerably greater contrast in its angular velocity with latitude than attained in these simulations. At odds with the solar data, too, is the large amplitude of the meridional circulation. In such local *f*-plane models, there is no restraint on the north-south flow given the lateral periodic boundary conditions, and thus by coupling via the Coriolis terms of the mean equations, the zonal and meridional flows are of comparable amplitude. In the correct spherical geometry, the meridional flows are probably decelerated by convergence of flows at the poles (and possibly the equator). The local nature of the model does not take this into account and thus probably overemphasizes the importance of the meridional flows. No such convergence deceleration exists for the zonal flows, and thus the results here for that component may well be more robust.

The mean flows are time-dependent, exhibiting prominent inertial oscillations, but when these effects are filtered out, the remaining time-averaged mean flows typically display a spiralling in the vector sum of their components with depth. This result is akin to deductions from ring diagram analyses of helioseismic data (e.g., Patron et al. 1995; Thompson et al. 1996) which reveal that a moderate mean flow exists below the solar surface whose direction appears to spiral with depth. The current simulations suggest that such spiralling arises from rotating boundary layer effects and may be indirectly linked to the nature of plume or coherent structure formation under the influence of rotation. Convergent motions required to form downflows at the upper surface necessarily spin up cyclonically, which, coupled with the compressible expansion of upflows in these stratified layers, yields positive helicity near the upper boundary, similar to the handedness of the spirals. The nature of the mean helicity profile here, being generally positive in the upper portions of the layer and negative in the lower, fulfils a necessary requirement for the success of some current solar magnetic field dynamo models. Interface dynamo theory has suggested that regions of negative helicity and positive radial shear of the mean zonal momentum must coincide, or be closely coupled, at the base of the convection zone in order to reproduce the observed migration of sunspots toward the equator (e.g., Stix 1991; Weiss 1994). The mechanisms suggested by these *f*-plane simulations for the production of shear and helicity at the lower surface appear to be robust for most boundary conditions. All that is required is that there be a deceleration of the convective plumes or coherent structures as they approach the boundary and a local conservation of angular momentum under the rotational influence for plumes leaving a boundary.

The inclusion of sufficient degrees of freedom, made possible by the local nature of the *f*-plane domain, has made it feasible to study of the interaction of fully turbulent convection under the effects of rotation. This has revealed features in the resulting mean zonal flows that bear some interesting similarity to aspects of solar observations. Such results encourage work toward more realistic global spherical shell modeling of convection that can encompass fully turbulent regimes.

The authors thank John Hart, Keith Julien, Mark Rast, Steve Tobias, and Joseph Werne for helpful discussions and Fausto Cattaneo for his part in originating the numerical code and for many useful conversations. Computations were carried out on the Cray C-90 at the Pittsburgh Supercomputing Center (PSC) under grant MCA93S005P and on the Kendall Square Research KSR-1 at the University of Colorado. We thank Paul Puglielli and Raghurama Reddy at PSC and Clive Baillie and Xin Xie for help in transferring the code to the KSR. This work was partially supported by the National Science Foundation through grants ESC-9217394 and AST 94-17337, by NASA through grants NAG 5-2256, NAG 5-3077, NAS 8-39747, and NCCS 5-157, and through Lockheed Martin Independent Research Funds.

REFERENCES

Batchelor, G. K. 1967, An Introduction to Fluid Dynamics (Cambridge: Cambridge Univ. Press)
Bodgan, T. J., Cattaneo, F., & Malagoli, A. 1994, ApJ, 407, 316
Brown, T. M., Christensen-Dalsgaard, J., Dziembowski, W. A., Goode, P. R., Gough, D. O., & Morrow, C. A. 1989, ApJ, 242, 526
Brummell, N. H., Cattaneo, F., & Toomre, J. 1995, Science, 269, 1370
Brummell, N. H., Hurlburt, N. E., & Toomre, J. 1996, ApJ, 473, 494 (Paper I)
Brummell, N. H., & Julien, K. 1997, preprint
Castaing, B., et al. 1989, J. Fluid Mech., 204, 1
Cattaneo, F., Brummell, N. H., Toomre, J., Malagoli, A., & Hurlburt, N. E. 1991, ApJ, 370, 282
Clune, T., Brummell, N. H., & Toomre, J. 1997, preprint
DeLuca, E. E., Werne, J., Rosner, R., & Cattaneo, F. 1990, Phys. Rev. Lett., 64, 2370
Gilman, P. A., & Miller, J. 1986, ApJS, 61, 585
Glatzmaier, G. A. 1987, in The Internal Solar Angular Velocity, ed. B. R. Durney & S. Sofia (Dordrecht: Reidel), 263
Gough, D. O., Leibacher, J. W., Scherrer, P. H., & Toomre, J. 1996, Science, 272, 1281
Gough, D. O., & Toomre J. 1991, ARA&A, 29, 627
Hathaway, D. H., Gilman P. A., & Toomre J. 1979, Geophys. Astrophys. Fluid Dyn., 13, 289.
Hathaway, D. H., & Somerville, R. C. J. 1986, J. Fluid Mech., 164, 91
Hathaway, D. H., Toomre, J., & Gilman, P. A. 1980, Geophys. Astrophys. Fluid Dyn., 15, 7
Heslot, F., Castaing, B., & Libchaber, A. 1987, Phys. Rev. A, 36, 5870
Howard, L., & Krishnamurti, R. 1986, J. Fluid Mech., 170, 385
Hurlburt, N. E., Toomre, J., & Massaguer, J. M. 1984, ApJ, 282, 557
Julien, K., Legg, S., McWilliams, J., & Werne, J. 1997, preprint
Libbrecht, K. G. 1989, ApJ, 336, 1092
Patron, J., Hill, F., Rhodes, E. J., Jr., Korzennik, S. G., & Cacciani, A. 1995, ApJ, 455, 746
Pedlosky, J. 1979, Geophysical Fluid Dynamics (Berlin: Springer)
Porter, D. H., Pouquet, A., & Woodward, P. R. 1994, Phys. Fluids, 6, 2133
Rucklidge, A. M., & Matthews, P. C. 1993, in Solar and Planetary Dynamos, ed. M. R. E. Proctor, P. C. Matthews, & A. M. Rucklidge (Cambridge: Cambridge Univ. Press), 257
She, Z.-S., Jackson, E., & Orszag, S. 1990, Nature, 344, 226
Spiegel, E. A., & Zahn, J.-P. 1992, A&A, 265, 106
Stix, M. 1991, Geophys. Astrophys. Fluid Dyn., 62, 211
Thompson, M., et al. 1996, Science, 272, 1300
Tomczyk, S., Schou, J., & Thompson, M. J. 1995, ApJ, 448, L57
Vincent, A., & Meneguzzi, M. 1991, J. Fluid Mech., 225, 1
Weiss, N. O. 1994, in Lectures on Solar and Planetary Dynamos, ed. M. R. E. Proctor & A. D. Gilbert (Cambridge: Cambridge Univ. Press), 59
Werne, J. 1993, Phys. Rev. E, 48, 1020
Werne, J., DeLuca, E. E., Rosner, R., & Cattaneo, F. 1991, Phys. Rev. Lett., 67, 3519

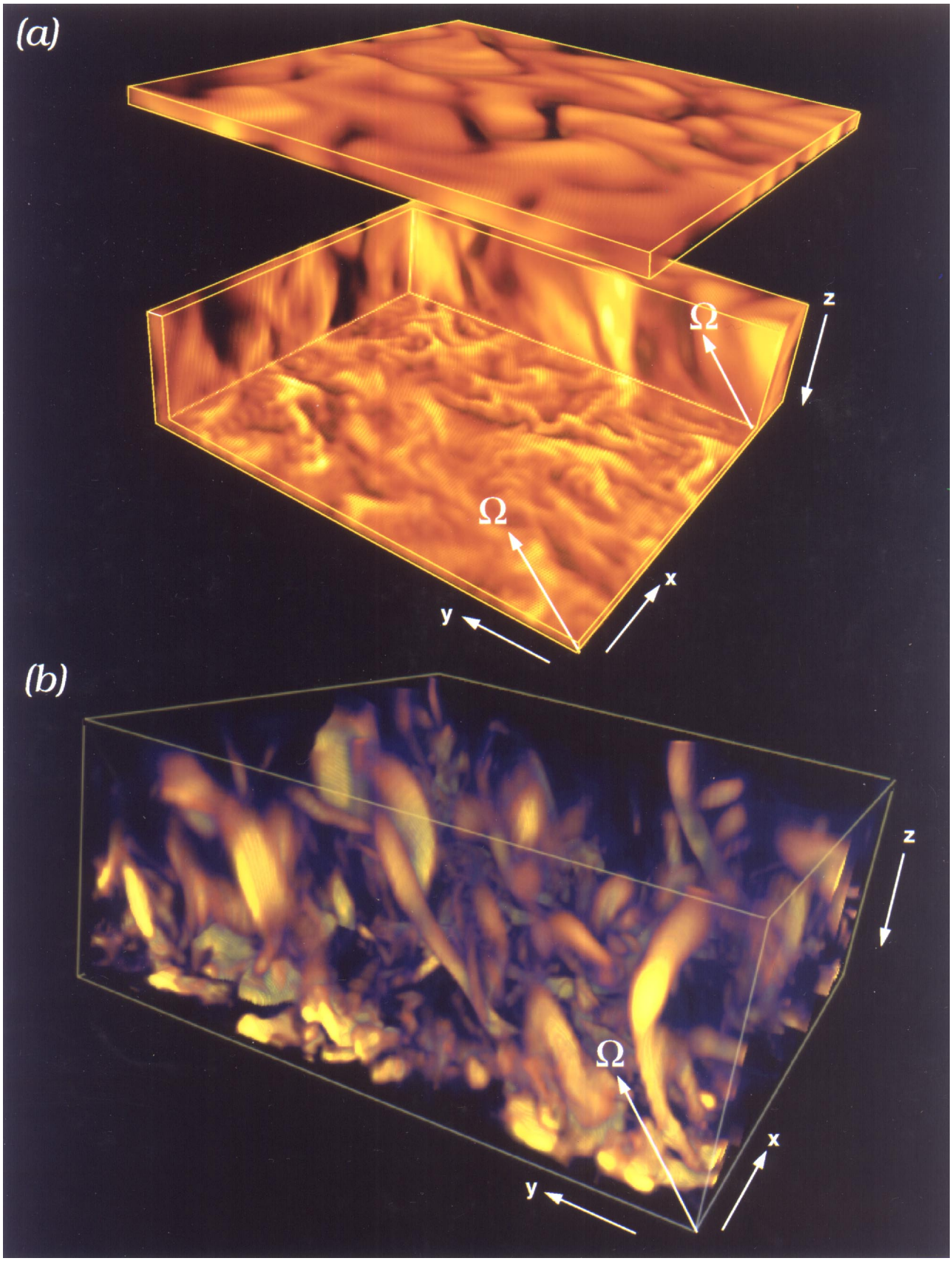

FIG. 2.—(*a*) The computational domain of case R4 is shown in vertical velocity at one instant in time, with dark (black and deep red) colors exhibiting downflow and light (yellow and white) tones show upflow. A layer near the upper surface has been moved away from the domain, and a section of the interior has been cut away. The smooth cellular surface contrasts with the smaller scale turbulent interior, as exhibited by the visible horizontal planes. On the vertical planes, vertical flows can be seen spanning the whole depth that tend to align with the rotation in the *y*-*z* plane and yet show no particular organization in the *x*-*z* plane. (*b*) The same case shown in enstrophy (vorticity squared) where bright (white and yellow) and opaque portions have high enstrophy, and dark (purple and blue) and translucent regions are low vorticity. Strong downflowing vortical coherent structures can again be seen aligned with the rotation vector.

BRUMMELL, HURLBURT, & TOOMRE (see 493, 958)